Research Article

SOHAG JOURNAL OF SCIENCES

https://doi.org/10.21608/sjsci.2025.383199.1271

Synthesis and characterization of $La_{0.6}Sr_{0.4}Mn_{0.8}Co_{0.2}O_3$ nanoparticles

M. A. Awad[1], Abdalrahman M. Rayan[1], A. A. Azab[2], I. A. Abdel-Latif[3], Mahrous R. Ahmed[1,*]

[1] *Physics Department, Faculty of Science, Sohag University, 82524 Sohag, Egypt.*
[2] *Solid State Physics Department, Physics Research Institute, National Research Center, Dokki, Giza, 12622, Egypt.*
[3] *Department of Reactor Physics, NRC, Egyptian Atomic Energy Authority, Cairo, Egypt.*
[*] *Email: Mahrous.r.ahmed@science.sohag.edu.eg*

Received: 8th May 2025, **Revised:** 30th May 2025, **Accepted:** 22nd June 2025
Published online: 9th August 2025

Abstract: $La_{0.6}Sr_{0.4}Mn_{0.8}Co_{0.2}O_3$ nanoparticles were synthesized by the sol-gel method. X-ray diffraction and Rietveld refinement confirmed the hexagonal perovskite structure. The output of Rietveld refinement provided detailed information about the crystal structure and facilitated the accurate crystallite size determination. Using the size strain model, the crystallite size and microstrain were calculated to be 15.15 nm and 0.00013, respectively. Fourier transform infrared spectroscopy supported the perovskite structure through the characteristic absorption bands in the low wavenumber range. A scanning electron microscope revealed the formation of aggregated nanoparticles with sizes exceeding the crystallite size. The electrical conductivity confirmed the semiconducting behavior, where the Arrhenius plot confirmed the presence of two activation energies, $Ea_1 \approx 0.07$ eV and $Ea_2 \approx 0.26$ eV. The vibrating sample magnetometer measurement indicated the presence of competing exchange interactions responsible for unsaturated magnetization that induce the formation of superparamagnetic-like behavior at room temperature. These findings suggest the potential of using $La_{0.6}Sr_{0.4}Mn_{0.8}Co_{0.2}O_3$ nanoparticles in applications such as biomedical fields and in spintronic devices.

Keywords: $La_{0.6}Sr_{0.4}Mn_{0.8}Co_{0.2}O_3$, X-ray, Rietveld refinement, Scanning electron microscope, Electric conductivity, superparamagnetic-like behavior.

1. Introduction

In recent decades, the discovery of superparamagnetic activity in nanoscale magnetic materials has gained a lot of attention due to its potential use in a wide range of complex applications. This phenomenon is characterized by the absence of magnetic hysteresis and remanence, unlike ferromagnetic materials, which possess a hysteresis behavior [1]. Those superpara-magnetic materials are particularly beneficial for applications in spintronics [2], energy storage [3], and biomedical fields [4, 5].

Among these advanced materials, perovskite-type oxides with the general formula LSMO nanoparticles have attracted increasing attention due to their remarkable electrical, magnetic, and structural properties[6,7]. These invaluable properties originate from the substitution of La^{3+} with Sr^{2+}, which induces the formation of mixed-valence states of Mn^{4+} and Mn^{3+}, inducing the double exchange interactions, hence enhancing the electrical conductivity and magnetic ordering[8,11]. Despite these fascinating properties, LSMO NPs possess a large hysteresis loop and saturation magnetization[12,13], which are not efficient in modern applications[4,5]. Recently, the introduction of Co modifies the magnetic properties of LSMO nanoparticles by enhancing superexchange interactions that oppose the double exchange interactions[8]. This, in turn, decreases the saturation magnetization and facilitates the transition of LSMO nanoparticles to superparamagnetic at room temperature[6-14,16]. On the other hand, the partial substitution of Mn with Co alters the electronic band width of LSMOs nanoparticles [17]. These effects contribute to the development of materials with promising characteristics for advanced technologies [18,20].

This work aims to synthesize LSMCO nanoparticles using the sol-gel method. The sol-gel method is characterized by low price and precise control in size, shape, and stoichiometry [21]. The structural properties of the resulting perovskite were investigated by Rietveld refinement and supported by FTIR analysis. The output of Rietveld refinement was used to extract the structural parameters and to accurately calculate the crystallite size. The magnetic behavior showed a very narrow hysteresis loop with unsaturated magnetization that indicated the formation of superparamagnetic behavior. The characteristics indicate the potential of LSMCO nanoparticles for various advanced applications, especially in the biomedical field.

2. Materials and methods

Perovskite LSMCO NPs were synthesized by the sol-gel method using nitrate salts, Lanthanum Nitrate Hexahydrate ($La(NO_3).6H_2O$), Strontium Nitrate ($Sr(NO_3)_2$) and Manganese Nitrate ($Mn(NO_3)_2$) which were purchased from Sigma Aldrich with high purity (99.99% purity) and Cobalt Nitrate Hexahydrated ($Co(NO_3)_2.6H_2O$) from Alpha chemical (99% purity). The stoichiometric composition of $La_{0.6}Sr_{0.4}Mn_{0.8}Co_{0.2}O_3$ was created by combining the necessary precursor weights in 100 mL of deionized water and then adding 0.01 mole of citric acid to the mixture. The solution was then agitated constantly for 30 min at 80°C to create a clear, light pink solution. Ammonia solution was added to

adjust the pH to a value of 9, and then the solution was stirred for two h to ensure solubility. The solution was dried in a drying furnace at 105°C for 36 h. Finally, the dried gel was calcined at 700°C for 8 h before being ground for 30 min using a mortar. Fig. 1 illustrates the reaction steps for preparing LSMCO nanoparticles.

X-ray diffraction (XRD) analysis, which is a powerful tool in crystal phase identification[22,23], was performed using a Bruker D8-Advance X-ray diffractometer equipped with a CuKα_1 (1.5406 Å) radiation source. The diffraction data were collected at room temperature over an angular range of 2θ = 20° to 80° with a step width of 0.02° to determine the crystal structure and phase purity. Fourier Transform Infrared (FTIR) spectroscopy was carried out utilizing a Bruker Alpha Platinum ATR spectrometer in the 4000-400 cm spectral range.

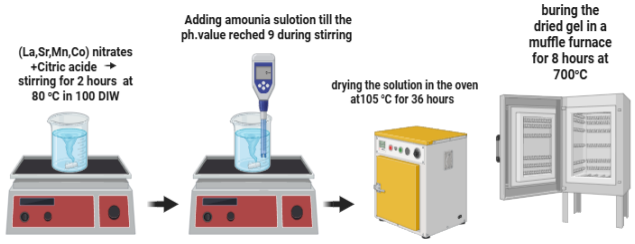

Figure 1: The reaction steps to synthesize LSMCO nanoparticles

A Vibrating Sample Magnetometer (VSM-7410, Lake Shore) was used to detect magnetization as a function of magnetic field (M-H) at room temperature, and a scanning electron microscope (SEM, Zeiss LEO Supra 35VP, maximum electron energy 30 keV) was used to evaluate surface morphology.
The electrical properties were measured using a stainless-steel cryostat under vacuum at a pressure of 10^{-3} mbar using an Edwards two-stage rotary vane pump. The voltage and current values were recorded using a UT71E high-accuracy digital multimeter and a DC power supply from Impo Electronics DC power supply. The temperature was precisely controlled using a PID temperature controller (TCN4S-24R) in conjunction with a chromel-alumel thermocouple.

3. Results and Discussion

3.1. Structural analysis and crystallite size calculation

The crystal structure of LSMCO nanoparticles calcinated at 700°C, as presented in Fig. 2, matches well with the crystallography database of the hexagonal phase of LSMCO (COD 4002478). Only minor diffracted peaks corresponding to secondary phases of $SrCO_3$ (COD 9013802) at 2θ = 25.18, 25.56, 30, 36.1, and 44° are observed. The reason may be because calcination temperature is carried out at atmospheric pressure, containing CO_2 gas that carbonates strontium-containing compounds, forming a layer containing $SrCO_3$ [24]. Goldschmidt tolerance factor [25] were computed to examine the formation of the perovskite structure. Mainly, the tolerance factor (t) is a dimensionless parameter used to predict the stability and distortion of perovskite structures (general formula ABX_3, where A and B are cations, and X is an anion). The following equation states the tolerance factor formula:

$$t = \frac{r_A + r_X}{\sqrt{2}\,(r_B + r_X)} \quad (1)$$

Where r_A is the ionic radius of the A-site atom, r_B is the ionic radius of the B-site atom, and r_X is the ionic radius of the anion. In our study, the A-site is occupied by Lanthanum or strontium, for the B-site, it is occupied by manganese or cobalt, and the anion is oxygen. The value of ionic radii for the atoms is given in Table 1.

Table 1: The value of ionic radii for the atoms of our compound.

Atom	Ionic radius (Å)	
Lathanum	1.061 Å	
Stronium	1.12 Å	
Manganses	Mn^{+3}	Mn^{+4}
	0.70 Å	0.62 Å
Cobalt	Co^{2+}	Co^{3+}
	0.745 Å	0.56 Å
Oxygen	1.40 Å	

It's known that Mn exhibits multiple oxidation states (+2, +3, +4, +6, +7), and each oxidation state influences the ionic radius. But in our case, only Mn^{+3} and Mn^{+4} form the prevoksite structure. The origin of the studied compound is $LaMnO_3$, with a reported tolerance factor, introducing atoms such as strontium or cobalt as a dopant . The Rietveld refinement was performed to confirm the hexagonal structure and to determine the structural parameters[1]. Pseudo-Voigt function is employed in the fitting process[26] Fig. 3 presents the refinement results that show good fitting between experimental and theoretical data, with a reliability factor of χ^2 = 1.35.

Table 2 summarizes the structural parameters, atomic positions, occupancy, bond lengths, and bond angles of LSMCO nanoparticles calcinated at 700°C. The VESTA software was utilized to illustrate the hexagonal lattice of LSMCO nanoparticles (Fig. 4), with red spheres signifying O atoms, and purple and green spheres signifying Mn/Co and Sr/La atoms, respectively. The exchange of A and B site atoms arises from the proximity of their ionic radii within the perovskite structure [27[. Figure 5b shows the supercell structure of LSMCO nanoparticles, which highlights the favored orientation along the (104) plane as revealed by the XRD pattern.
The crystallite size calculations of LSMCO have been investigated from the refined FWHM values, where these values have been corrected by eliminating broadening due to the diffractometer contribution using the following equation:

$$\beta_{(corrected)} = (\beta^2_{refined} - \beta^2_{diffractometer})^{1/2} \quad (2)$$

where $\beta_{(corrected)}$ is the FWHM after eliminating the diffractometer broadening, $\beta_{(refined)}$ is the value of the FWHM obtained from the Rietveld refinement, and $\beta_{(diffractometer)}$ is the FWHM obtained after substitution in the polynomial obtained from the resolution profile. The size-strain plot (SSP) is used to calculate crystallite size and microstrain (Fig. 5. This model assumes the peak broadening in XRD due to crystallite size and microstrain, where the line broadening data is transformed

into a linear fit from which crystallite size and microstrain are extracted according to[28]:

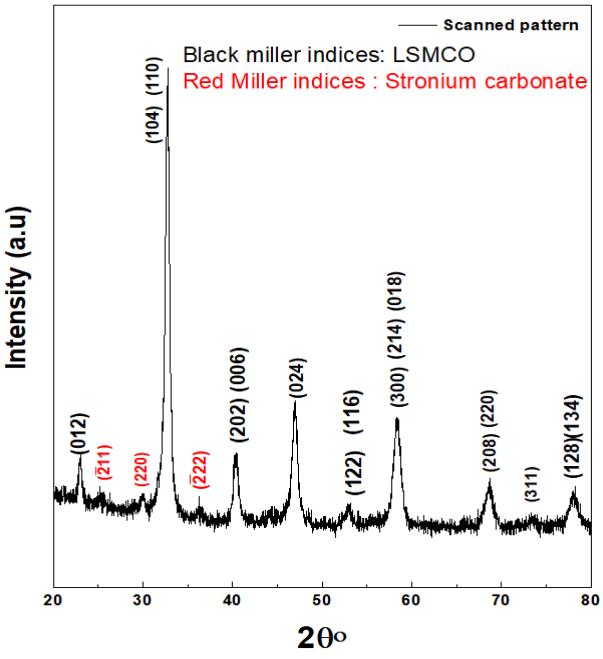

Figure 2: XRD of LSMCO NPs calcinated at 700°C

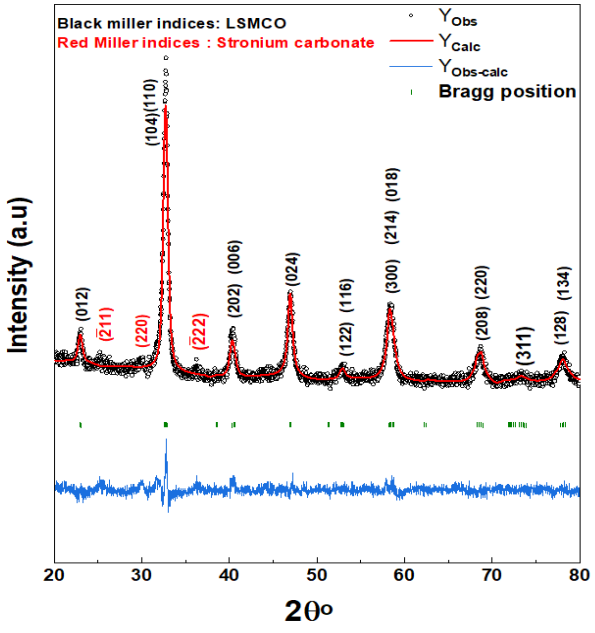

Figure 3: Reitveld refinement of LSMCO NPs calcinated at 700°C.

$$(d_{hkl}\beta_s \mathrm{Cos}\,\theta_{hkl})^2 = \frac{k\lambda}{D}(d^2_{hkl}\beta_s \mathrm{Cos}\,\theta_{hkl}) + (\frac{\varepsilon\lambda}{2})^2 \quad (3)$$

where d_{hkl} represents the d-spacing for the refined XRD peaks, β_{hkl} refers to the corrected FWHM, K is the shape factor that depends on crystallite size and shape, D is the crystallite size, and ε is the macrostrain. By plotting $(d_{hkl}\beta_{hkl}\mathrm{Cos}\,\theta_{hkl})^2$ on the Y axis and $(d^2_{hkl}\beta_{hkl}\mathrm{Cos}\theta_{hkl})$ on the X-axis, the crystallite size is calculated from the slope and the microstrain from the intercept according to:

Table 2: The structural parameters, atomic positions, occupancy, bond lengths, and bond angles of LSMCO nanoparticles calcinated at 700 °C.

Structural parameters		Atomic positions and occupancies			Bond length and angle	
Crystal system	Hexagonal	Atom	(x,y,z)	Occupancy	(Mn/Co - O)	1.94677 Å
Space group	R -3 c	La	(0,0,0.25)	0.59128	(Mn/Co - O – Mn/co)	167.6407°
Goodness of fitting	1.35	Sr	(0,0,0.25)	0.39985	(La/Sr – O)	2.74009 Å
R-factors	R_p:30 R_{wp}:22.9 R_{exp}:19.70	Mn	(0,0,0)	0.79980	(La/Sr - O – La/Sr)	171.2275°
Volume	348.0034 Å^3	Co	(0,0,0)	0.24438		
Lattice parameters	a = 5.4845 Å b =5.4845 Å c =13.3593 Å α = β = 90° γ = 120°	O	(0.46179,0,0.25)	2.23847		

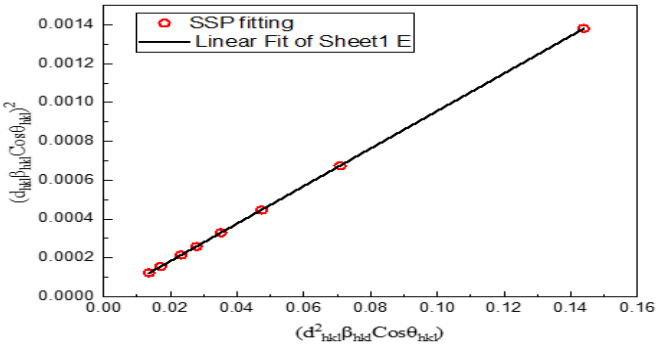

Figure 4: The unit cell and the supercell structure of LSMCO nanoparticles calcinated at 700°C.

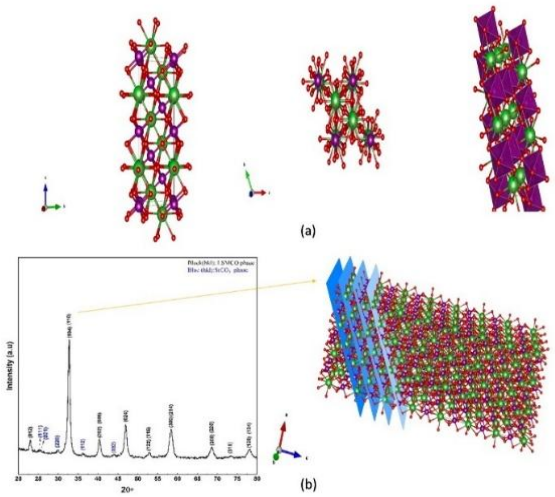

Figure 5: The size strain plot of LSMCO NPs calcinated at 700°C

$$\varepsilon = \frac{2\sqrt{intercept}}{\lambda} \quad (4)$$

The calculated crystallite of the LSMCO nanoparticles is 15.15 nm with an effective lattice strain of 0.00013, where the negative value indicates compressive microstrain.

3.2 The morphological and molecular analysis

A scanning electron microscope (Fig. 6) was used to indicate the surface morphology of LSMCO NPs. Obviously, the images show non-uniform and aggregated nanoparticles. The large particle size observed in the SEM images (around 20 µm) compared to the crystallite size estimated from the XRD analysis is caused by opposite magnetic dipole interactions. The particles clustering during the calcination process is an inherent characteristic of the perovskite, and it is consistent with previously mentioned behavior [29].

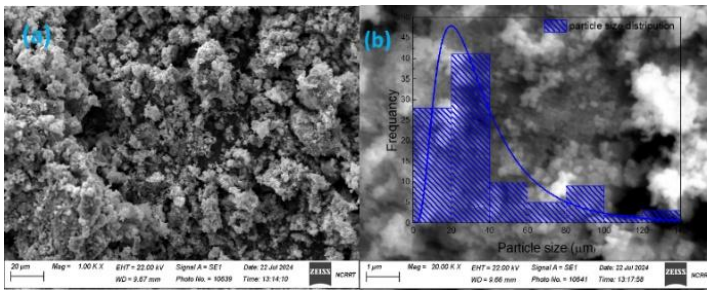

Figure 6: SEM of LSMCO NPs calcinated at 700°C

FTIR analysis is conducted to identify the functional groups and to confirm the presence of the perovskite structure. From Fig. 7, it is observed that the presence of several absorption bands, where the absorption band around 420 and 602 cm^{-1} corresponds to the stretching of the metal-oxygen bond in the perovskite structure [30,31]. The light shift in the absorption band compared to previously reported [32] reflects the internal change in the (Mn/Co - O - Mn/Co) bond length due to the incorporation of Co atoms into the site of Mn in the prevoskite structure. The absorption bands around 860 and 1060 cm^{-1} confirm the presence of carbonate functional groups [33], in agreement with the XRD results. The absorption bands around 1390, 1455, and 1630 cm^{-1} are indicative of the presence of minor retention of carbonyl groups (COO^-) [34] after calcination. The absorption bands around 2850 cm^{-1} and 2929 cm^{-1} are related to the presence of C-H stretching vibrations of $-CH_2$ and $-CH_3$ groups [34]. Finally, the absorption bands around 3150 and 3420 cm^{-1} correspond to the stretching vibrations of the O-H groups as a result of water molecule adsorption [35].

3.3 Magnetic and electrical properties

The magnetic behavior at room temperature of LSMCO nanoparticles at a calcination temperature of 700°C is represented in Fig. 8. It is observed that the presence of mini hysteresis-like behavior with no saturation magnetization. The reason relies on the presence of different magnetic dipoles that interact oppositely in the structure when applying the magnetic field. The double exchange interaction through electron transfer between Mn ions, such as Mn^{+3} to Mn^{+4} via O^{2-} ion [8], and the super exchange interaction originated from the Co presence in the structure (Co^{3+} - O^{2-} - Co^{3+} ions) and (Co^{4+} - O^{2-} - $Co^{4)}$ [8-17]. Where Co ions replace Mn ions due to the similarities of ionic radii [27] and decrease the Mn/Co-O-Mn/Co bond length compared to the LSMO structure [27]. This state of opposite dipole interactions inhibits the saturation magnetization, induces antiferromagnetic interaction [36,37], and shifts the hysteresis loop from its origin [38]. Although the ratio of the $SrCO_3$ secondary phase is small, it has an impact on the magnetic properties, where it can retain small retentivity indicated in the hysteresis loop. The result produces a superparamagnetic-like free spin system [6], which may be crucial for medical applications.

The electrical conductivity of LSMCO NPs was investigated in the temperature range from 300 to 460 K using two-terminal

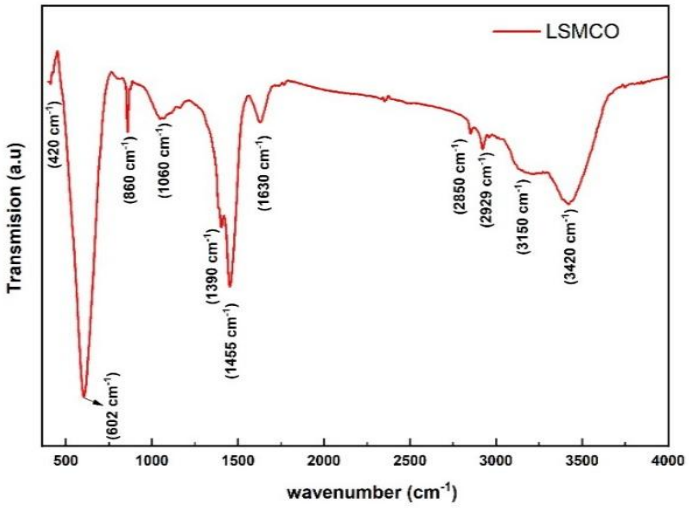

Figure 7: FTIR spectra of LSMCO NPs calcinated at 700°C

configurations (Fig. 9). Obviously, the conductivity increases with increasing temperature, denoting the semiconducting behavior. For deep insight into the magnetic behavior, the activation energy (E_a) is calculated using the Arrhenius plot

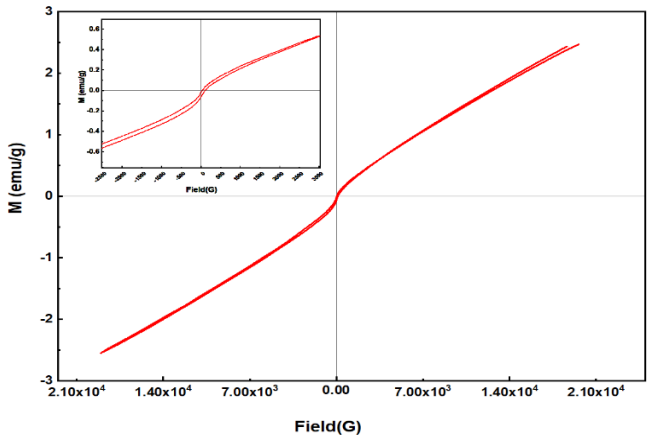

Figure 8: The magnetic behavior of LSMCO NPs calcinated at 700°C.

given by:

$$\sigma\,(T) = \sigma_o\, e^{\frac{-E_a}{K_B T}} \qquad (5)$$

where σ (T) represents the electrical conductivity, K_B is the Boltzmann constant, and T is the temperature in Kelvin.

It is clear from Fig. 10 that there are two distinct slopes, indicating the presence of two activation energies, Ea_1 = 0.07 eV at low temperature and Ea_2 = 0.26 eV at high temperature.

According torence Zener [39] $LaMnO_3$ behaves as a pure insulator at low temperatures. When Sr^{2+} ions substitute some of the La^{3+} sites in the LSMO unit cell, Mn^{4+} ions are formed in addition to Mn^{+3} ions. This mixed valence state facilitates the double exchange interaction, hence increasing the electrical conductivity in the low temperature range (Ea1).

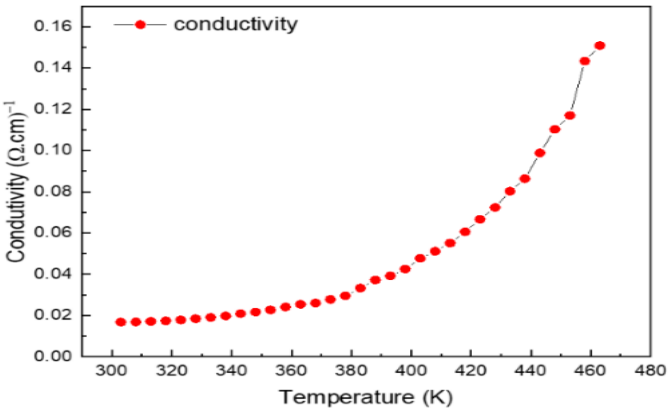

Figure 9: The electrical conductivity of LSMCO NPs calcinated at 700°C.

On the other hand, the activation energy in the high temperature range (Ea_2 = 0.26 eV) is due to the existence of Co^{+3} ions in substitution with Mn^{+3} ions, which decrease the ionic radii between cobalt-oxygen ions (d_{Co-O}) [40]. This decrement indicates a strong columb attraction between the electrons and cobalt nuclei. Additionally, the phase separation of $SrCO_3$ contributes to this high Ea2 value by free carrier trapping [41]. For these reasons, the second activation energy is much higher than the first one. Similar values of our activation energies are reported elsewhere[42].

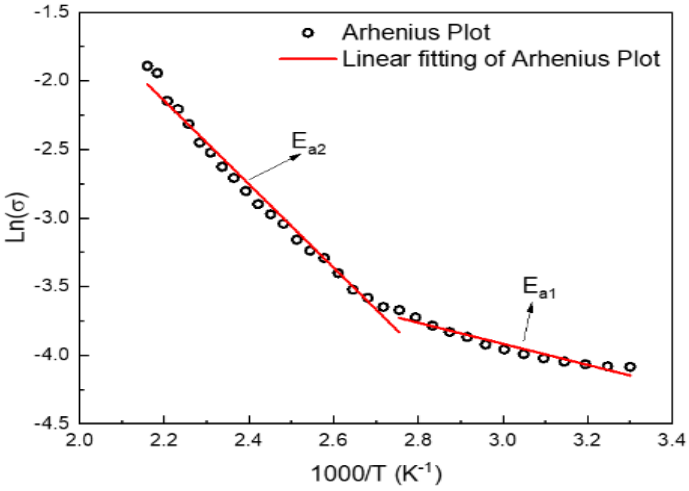

Figure 10: The Arrhenius fitting of LSMCO NPs calcinated at 700°C.

4. Conclusion

The perovskite structure of LSMCO nanoparticles was synthesized using the sol-gel technique and subsequently calcined at 700 °C. Structural analysis by Rietveld refinement facilitated the extraction of the structural parameters and the precise estimation of crystallite size through the size-strain model. The magnetic behavior demonstrated the emergence of unsaturated magnetization, which indicates the presence of opposite spin interactions between double exchange and superexchange interactions. The electrical study revealed the semiconducting behavior, with two activation energies extracted from the Arrhenius plot. These findings highlight the possibility of using LSMCO nanoparticles in many applications, such as biological and spintronic technology.

CRediT authorship contribution statement:

Conceptualization has been done by Mahrous R. Ahmed, I. A. Abdel-Latif, M. A. Awad and Abdelrahman M. Rayan; methodology has been carried out by Abdelrahman M. Rayan and M. A. Awad; software has been carried out by Abdelrahman M. Rayan; validation has been done by M. A. Awad and Abdelrahman M. Rayan; resources has been carried out by Mahrous R. Ahmed and Abdelrahman M. Rayan; data curation has been carried out by M. A. Awad and Abdelrahman M. Rayan; writing- original draft preparation has been carried out by M. A. Awad and Abdelrahman M. Rayan; review and editing has been carried out by M. A. Awad; Mahrous R. Ahmed, I . A. Abdel-Latif; visualization has been carried out by Mahrous R. Ahmed, I. A. Abdel-Latif, M. A. Awad and Abdelrahman M. Rayan; supervision has been carried out by Mahrous R. Ahmed; I. A. Abdel-Latif and M. A. Awad; All authors have read and agreed to the published version of the manuscript

Data availability statement

The data used to support the findings of this study are available from the corresponding author upon request.

Declaration of competing interest

The authors declare that they have no known competing financial interests or personal relationships that could have appeared to influence the work reported in this paper.

Acknowledgments

The Authors gratefully thank the University of Sohag for funding this work.

References

[1] M.R. Ahmed, E. Ibrahim, A. Hamazaoui, A.M. Rayan, A. Azab, A.A.J.P.S. Hakeem, *Journal of Power Sources*, 99 (2024) 115905.
[2] S. Martin-Rio, Z. Konstantinovic, A. Pomar, L. Balcells, J. Pablo-Navarro, M.R. Ibarra, C. Magén, N. Mestres, C. Frontera, B.J.A.a.m. Martínez, *ACS Applied Materials & Interfaces*, 15 (2023) 37038-37046.
[3] J. Zheng, H. Zhao, X. Guo, X. Jin, L. Wang, S. Dong, J.J.C. Chen, *Ceramics International*, 14 (2023) 20.
[4] N. Sezer, İ. Arı, Y. Biçer, M.J.J.o.M. Koç, *Journal of Materials*, 538 (2021) 168300.
[5] V.M. Kulkarni, D. Bodas, K.M.J.R.A. Paknikar, *Royal Society of Chemistry Advances*, 5 (2015) 60254-60263.
[6] X. Chen, J. Fu, C. Yun, H. Zhao, Y. Yang, H. Du, J. Han, C. Wang, S. Liu, Y.J.J.o.a.p. Zhang, *Journal of Applied Physics*, 116 (2014) 053907.
[7] M.R.J.J.o.M. Ahmed, *Journal of Magnetism and Magnetic* Materials, 504 (2020) 166628.
[8] C.J.P.R. Zener, *Physical Review*, 82 (1951) 403.
[9] M.R. Ahmed, G.J.P.R.B.C.M. Gehring, *Physical Review B*, 74 (2006) 014420.
[10] M.R. Ahmed, G.J.P.R.B.C.M. Gehring, *Physical Review B*, 79 (2009) 174106.
[11] I. Abdel-Latif, M.R. Ahmed, I. Al-Omari, A.J.J.o.M. Sellai, *Journal of Magnetism and Magnetic Materials*, 420 (2016) 363-370.
[12] J.N. Dahal, D. Neupane, T.J.A.A. Poudel, *Applied Acoustics*, 9 (2019) 103233.
[13] H. Das, A. Inukai, N. Debnath, T. Kawaguchi, N. Sakamoto, S.M. Hoque, H. Aono, K. Shinozaki, H. Suzuki, N.J.J.o.P. Wakiya, *Journal of Physics and Chemistry of Solids*, 112 (2018) 179-184.
[14] M.R. Ahmed, A.M. Ahmed, A. Diab, S.J.S.J.o.S. Abo-Elhasan, *Surfaces and Interfaces*, 7 (2022) 9-14.
[15] A. Kurbakov, I. Abdel-Latif, M.R. Ahmed, H. Habermeier, A. Al-Hajry, A. Malyshev, V. Ulyanov, T.M.J.T.E.P.J.P. El-Sherbini, *The European Physical Journal Plus*, 137 (2022) 658.
[16] H.F. Mohamed, A.M. Ahmed, M.R. Ahmed, J.A. Paixão, S.A.J.p.s.s. Mohamed, *Physica Status Solidi* (a), 260 (2023) 2300175.
[17] M. Itoh, I. Natori, S. Kubota, K.J.J.o.m. Motoya, *Journal of Magnetism and Magnetic Materials*, 140 (1995) 1811-1812.
[18] C. Moure, O. Peña, *Progress in Solid State Chemistry*, 43 (2015) 123-148.
[19] E.A.R. Assirey, *Saudi Pharmaceutical Journal*, 27 (2019) 817-829.
[20] L.G. Tejuca, J.L. Fierro, Properties and Applications of Perovskite-Type Oxides, *CRC Press*, 1992.
[21] J.D. Mackenzie, E.P.J.A.o.c.r. Bescher, *Accounts of Chemical Research*, 40 (2007) 810-818.
[22] A. El Abd, M. Taman, R. Behiry, M. El-Naggar, M. Eissa, A.M. Hassan, W.A. Bar, T. Mongy, M. Osman, A.J.C. Hassan, *Cement and Concrete Composites*, 449 (2024) 138436.
[23] P.S. Quinn, A.J.T.e.o.a.s. Benzonelli, *The Encyclopedia of Applied Spectroscopy*, (2018) 1796-1800.
[24] R. Sezer, E. Yilmaz, S. Ertürk, C. Arslan, Calcination of Strontium Carbonate in Rotary Kiln Furnace, *10th International Symposium on High-Temperature Metallurgical Processing*, Springer, 2019, pp. 591-597.
[25] C.J. Bartel, C. Sutton, B.R. Goldsmith, R. Ouyang, C.B. Musgrave, L.M. Ghiringhelli, M.J.S.a. Scheffler, *Science Advances*, 5 (2019) eaav0693.
[26] A.A. Alsimaree, A.M. Rayan, A.M. Almohyawi, M.A. Hassan, M.R. Ahmed, A. Timoumi, S.A.J.C.I. Ahmed, *Ceramics International*, (2025) in press.
[27] K.S. Ali, R. Saravanan, A. Pashchenko, V.J.J.o.A. Pashchenko, *Journal of Alloys and Compounds*, 501 (2010) 307-312.
[28] H.M. Abd El-Lateef, A.M. Rayan, A. Azab, M.R. Ahmed, M.A.J.J.o.M.S.M.i.E. Hassan, *Journal of Materials Science: Materials in Electronics*, 36 (2025) 419.
[29] S. Ravi, A.J.P.p. Karthikeyan, Physics Procedia, 54 (2014) 45-54.
[30] S. Ravi, A. Karthikeyan, *Physics Procedia*, 54 (2014) 45-54.
[31] Z. Razi, A. Khajehnezhad, *Plasmonics*, 18 (2023) 1885-1891.
[32] M. Bourguiba, Z. Raddaoui, M. Chafra, J.J.R.a. Dhahri, *RSC Advances*, 9 (2019) 42252-42261.
[33] W.-D. Yang, Y.-H. Chang, S.-H.J.J.o.t.E.C.S. Huang, *Journal of The Electrochemical Society*, 25 (2005) 3611-3618.
[34] W.S. Ham, M.K. Kim, J.S. Gim, J.S. Lee, J.H. Wu, K.B. Lee, Y.K.J.I.T.o.M. Kim, *IEEE Transactions on Magnetics*, 51 (2015) 1-4.
[35] W.S. Ham, M.K. Kim, J.S. Gim, J.S. Lee, J.H. Wu, K.B. Lee, Y.K. Kim, *IEEE Transactions on Magnetics*, 51 (2015) 1-4.
[36] N. Phuc, L. Bau, N. Khiem, L. Son, D.J.P.B.C.M. Nam, *Physica B: Condensed Matter*, 327 (2003) 177-182.
[37] H. Zhang, B. Xia, D.J.J.o.M. Gao, *Journal of Magnetism and Magnetic Materials*, 569 (2023) 170428.
[38] J. Nogués, J. Sort, V. Langlais, V. Skumryev, S. Suriñach, J. Muñoz, M.J.P.r. Baró, *Physics Reports*, 422 (2005) 65-117.
[39] C. Zener, *Physical Review*, 82 (1951) 403.
[40] C. Zener, *Physical Review*, 82 (1951) 403-405.
[41] M. Awad, A. Ahmed, V. Khavrus, E.J.C.I. Ibrahim, *Ceramics International*, 41 (2015) 10116-10124.
[42] T.L. Pham, J.H. Yu, J.-S.J.C. Lee, *ChemCatChem*, 11 (2021) 712.